



Highly efficient photocatalytic H₂ evolution over MoS₂/CdS-TiO₂ nanofibers prepared by an electrospinning mediated photodeposition method

Na Qin^a, Jinhua Xiong^a, Ruowen Liang^a, Yuhao Liu^a, Shiying Zhang^b, Yanhua Li^b, Zhaohui Li^{a,*}, Ling Wu^{a,*}

^a State Key Laboratory of Photocatalysis on Energy and Environment, Fuzhou University, Fuzhou 350002, PR China

^b Hunan Province Key Laboratory of Applied Environmental Photocatalysis, Changsha University, Changsha 410022, PR China

ARTICLE INFO

Article history:

Received 20 March 2016

Received in revised form 15 August 2016

Accepted 20 September 2016

Available online 20 September 2016

Keywords:

Electrospinning

Photodeposition

MoS₂/CdS-TiO₂ nanofibers

Interfacial contact

Photocatalytic H₂ evolution

ABSTRACT

MoS₂/CdS-TiO₂ nanofibers have been successfully prepared by an electrospinning mediated photodeposition method for improving the interfacial contact between MoS₂ and CdS-TiO₂ nanofibers. The structural features, morphologies, and photo-absorption performances of the as-prepared samples were investigated in detail. The photocatalytic activity of a typical sample 1%MoS₂/CdS-TiO₂(60) nanofibers for H₂ evolution under visible light irradiation exhibits 3.0 and 4.0 times higher than that of 1%MoS₂/CdS-P25(60) and 1%Pt/CdS-TiO₂(60), respectively. Based on the above results, it reveals that one dimensional TiO₂ nanofibers can serve as excellent substrates for improving the dispersion of CdS and MoS₂. Moreover, the intimate interaction among MoS₂, CdS and TiO₂ may be suggested by HRTEM images and elements mapping patterns. Further photoelectrochemical analyses show that the effective separation of photogenerated carriers can be markedly accelerated. Finally, a tentative photocatalytic reaction mechanism has also been investigated. This work demonstrates that the method of combining electrospinning and photodeposition is feasible for the preparation of an effective MoS₂/CdS-TiO₂ nanofibers composite photocatalyst.

© 2016 Elsevier B.V. All rights reserved.

1. Introduction

Photocatalytic H₂ production from water splitting is recognized as a green, economical, and promising way to convert sustainable solar energy into preservable H₂ [1–3]. So far, a great deal of photocatalysts including (oxy)nitrides, (oxy)sulfides, and metal oxides have been proved to be able to produce H₂ [4–7]. Among various candidates, CdS is an intriguing photocatalyst because of its narrow band gap (2.4 eV) for the excellent light absorption property, easy fabrication and a suitable conduction band edge for H₂ evolution reaction [8–10]. However, there still exist some problems in such semiconductor material, such as the rapid recombination of the photogenerated electron–hole pairs, and the CdS nanoparticles tendency to form agglomerates which would reduce its surface area and the available active sites for catalytic reactions [11,12]. Continuing efforts have been made to develop alternative approaches to further improve the H₂ evolution performance, including coupling

CdS with other semiconductors and cocatalysts [13–15], modulating the shape and morphology of CdS [16,17]. In principle, the difficulties can be solved by supporting the CdS nanoparticles on a substrate to prevent their coalescence, and the effective surface area of the CdS nanoparticles are still kept [18–20]. Recently, one dimensional (1D) TiO₂ such as nanotubes [21,22], nanorods [23] or nanofibers [24] is widely regarded as an superior substrate for the assembly of the other nanomaterials. In the synthesis methods of 1D TiO₂ materials, the electrospinning technique has become a commonly used way due to its simple and low-cost fabrication process [25,26]. Meanwhile, compared with P25 nanoparticles, it has some advantages of using electrospun TiO₂ nanofibers as supports due to that (i) the electrospun TiO₂ nanofibers possess 3D open structures, high porosity and large aspect ratios; (ii) the electrospun TiO₂ nanofibers can serve as outstanding substrates for the assembly of secondary nanostructures with high density without aggregation [24,27,28]. Furthermore, TiO₂ nanofibers are suitable support for CdS because of its matched conduction band position [29]. Hence, it's desirable to fabricate the CdS-TiO₂ nanofibers by dispersion of the CdS nanoparticles on the electrospun TiO₂ nanofibers.

* Corresponding authors.

E-mail address: wuling@fzu.edu.cn (L. Wu).

Besides the above, loading cocatalyst is also a typical and effective method to improve the separation of electron-hole pairs. Noble metals (such as Ru, Pd, Pt or Au) could be the efficient cocatalysts for CdS, but they are high cost [13,14]. It is desirable to explore highly efficient and low-cost noble-metal-free cocatalysts to further facilitate the development of H₂ evolution [30,31]. Recently, MoS₂ has attracted researchers' attention due to its excellent promotion for the photocatalytic H₂ production as well as its earth-abundant and high chemical stability [32–34]. It has also been reported that the interfacial contact between MoS₂ and reactant play an important role in the photocatalytic activity [7]. However, previous procedures for synthesizing MoS₂ have typically involved high temperature, long-time solvothermal treatment and reduction by toxic H₂S gas [35–37], which may limit their applications. Recently, some feasible procedures for synthesizing highly active MoS₂ catalysts are gradually rising [38]. Here we report that MoS₂ as a cocatalyst closely anchored on CdS-TiO₂ nanofibers are prepared by a facile way for boosting the photocatalytic H₂ production.

Herein, we report an electrospinning mediated photodeposition method to fabricate MoS₂/CdS-TiO₂ nanofibers. Firstly, CdS nanoparticles were grown on the electrospun TiO₂ nanofibers by a simple photodeposition method. Then, MoS₂ was photodeposited onto the CdS-TiO₂ nanofibers using (NH₄)₂MoS₄ as a precursor. The as-prepared 1%MoS₂/CdS-TiO₂ nanofibers exhibits much higher H₂ generation activity in lactic acid solution compared with 1%MoS₂/CdS-P25 composites and 1%Pt/CdS-TiO₂ nanofibers under visible light irradiation ($\lambda \geq 420$ nm). This is due to the following two reasons: (i) TiO₂ nanofibers can serve as excellent substrates for improving the dispersion of CdS and MoS₂; (ii) the formed interfacial contact among composites is beneficial to the transfer of photogenerated electrons during the photocatalysis.

2. Experimental section

All materials were used as received without further purification. Deionized water was obtained from local sources.

2.1. Preparation

2.1.1. Fabrication of CdS-TiO₂ nanofibers

Above all, TiO₂ nanofibers were prepared by an electrospinning method with post-calcination [39]. Firstly, 0.45 g PVP (Mw ≈ 1 300 000) was added to 7.5 mL of ethanol under vigorous stirring. Then, 1.5 g of titanium tetraisopropoxide was added to a mixed solution containing acetic acid (3 mL) and ethanol (3 mL), after stirring, added to the above solution. Subsequently, the mixture was transferred into a plastic syringe for electrospinning. Finally, the pure TiO₂ nanofibers were obtained by treating them in air at 500 °C for 3 h.

For the fabrication of CdS-TiO₂ nanofibers, the procedure was similar to the previous photodeposition method with a little modification [40]. At first, 50 mg of the TiO₂ nanofibers, 40 mg of CdCl₂·2.5H₂O and 10 mg of S₈ were dispersed in 15 mL of absolute ethanol to form a suspension. Then bubbled with N₂ for 30 min in the dark. At last, the suspension was irradiated by a 300 W Xe arc lamp without filter (300 < λ < 800 nm) for a given period ranging from 15, 30, 60, to 90 min. The samples were marked for CdS-TiO₂(15), CdS-TiO₂(30), CdS-TiO₂(60), CdS-TiO₂(90), respectively. The CdS-P25(60) composites were also prepared by the same photodeposition method just using P25 nanoparticles instead of TiO₂ nanofibers.

2.1.2. Preparation of MoS₂/CdS-TiO₂ nanofibers

The preparation of MoS₂/CdS-TiO₂ nanofibers was based on a facile photodeposition method [41–43]. 50 mg of the prepared CdS-TiO₂ nanofibers was first dispersed in a 20 mL mixture of

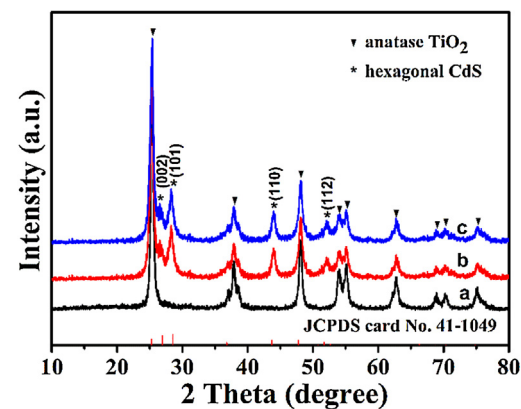


Fig. 1. XRD patterns of (a) TiO₂, (b) CdS-TiO₂(60) and (c) 1%MoS₂/CdS-TiO₂(60) nanofibers.

ethanol (5 mL) and distilled water (15 mL) that contained a certain amount of (NH₄)₂MoS₄ and then irradiated with a 300 W Xe lamp. N₂ was continuously bubbled through the sample solution before and during the irradiation to remove oxygen completely. Then, the products were separated by filtration, washed thoroughly with distilled water. Upon drying at 60 °C, the samples were obtained with different weight addition ratios of MoS₂, namely, 0.5%, 1%, 2%, 3%. 1%MoS₂/CdS-P25(60) composites were also prepared by the same method just using CdS-P25(60) composites instead of CdS-TiO₂(60) nanofibers. For comparison, 1%Pt/CdS-P25(60) composites and 1%Pt/CdS-TiO₂ nanofibers were prepared by a photodeposited method using H₂PtCl₆·6H₂O as the starting material.

2.2. Characterization

XRD patterns were collected on a Bruker D8 Advance X-ray diffractometer with Cu-K α radiation. The data were recorded in the 2θ range of 10–80°. ZEISS SIGMA scanning electron microscope (SEM) was used to determine the morphology of the samples. Transmission electron microscopy (TEM) and high-resolution transmission electron microscopy (HRTEM) analyses were recorded on a JEOL model JEM 2010 EX microscope, using an accelerating voltage of 200 kV. The concentration of Cd²⁺ was decided by the Ultima2 ICP optical emission spectrometer. UV-vis diffuse reflectance spectra (UV-vis DRS) were obtained using a UV-vis spectrophotometer (Varian Cary 500). X-ray photoelectron spectroscopy (XPS) measurements were operated on a Thermo Scientific ESCA Lab 250 instrument with a monochromatic Al K α source. The BET surface areas were carried out at 77 K on a Micromeritics ASAP 2020 apparatus. The photoluminescence (PL) spectra and the time-resolved fluorescence decay spectra were measured on an FLS 980 spectrophotometer (Edinburgh Analytical Instrument, UK). The photocurrent measurements were conducted on a BAS Epsilon workstation. A 300 W Xe lamp with a 420 nm cut-off filter was used as a light source. The electrochemical impedance spectroscopy (EIS) experiments were performed using a CHI660D workstation (CH instrument, USA).

2.3. Photoactivity test

The photocatalytic H₂ production tests were carried out in a Pyrex reaction cell connected to a closed gas circulation and evacuation system. The photocatalysts (20 mg) were dispersed in an 80 mL of 10 vol% lactic acid aqueous solution. The suspension was then thoroughly degassed, followed by irradiation with a 300 W Xe lamp (PLS-SXE300C, Perfectlight Co., Beijing) with a cut off filter

($\lambda \geq 420$ nm). The photon flux was 5.2×10^{17} s cm $^{-2}$ (the distance between the lamp and the reaction vessel was 10 cm; the irradiated area of the reactor is 31.2 cm 2). The amount of evolved H₂ was detected with an online gas chromatography. The apparent quantum efficiency (AQE) at 420 nm was conducted. The 300 W Xe lamp was used as the light source, and the number of incident photons was measured using a Si photodiode (ILT 950). The AQE was calculated by the following equation:

$$\text{AQE} = \frac{\text{Number of reacted electrons}}{\text{Number of incident photons}} \times 100\% \\ = \frac{\text{Number of evolved H}_2 \text{ molecules} \times 2}{\text{Number of incident photons}} \times 100\%$$

3. Results and discussion

3.1. Characterizations

The crystalline phases of the as-prepared samples were investigated by XRD. In Fig. 1, it can be seen that both CdS-TiO₂(60) and 1%MoS₂/CdS-TiO₂(60) samples possess analogous XRD patterns. Besides the typical diffraction peaks of anatase TiO₂ (JCPDS, No. 21-1272), the new diffraction peaks assigned to the hexagonal CdS (JCPDS, No. 41-1049) appear [40]. No typical diffraction peaks of MoS₂ are observed, which may be ascribed to the high dispersion and the low content of MoS₂ [44]. Moreover, Fig. S1 provides the XRD patterns of all CdS-TiO₂ samples with different deposition time.

UV-vis DRS spectra of the as-prepared samples are shown in Fig. 2. Compared with the sample of TiO₂, the CdS-TiO₂(60) sample displays a new visible absorption band, which corresponds to the light absorption edge of CdS [45]. After MoS₂ deposition, the UV-vis DRS of 1%MoS₂/CdS-TiO₂(60) shows obviously enhanced absorption over about 400 nm, which can be ascribed to the absorption of the narrow-band semiconductor MoS₂. In addition, for all the CdS-TiO₂ nanofibers, it is found that they exhibit enhanced absorption

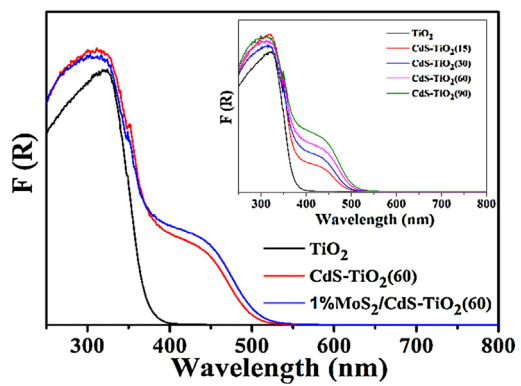


Fig. 2. UV-vis diffuse reflectance spectra of the pure TiO₂, CdS-TiO₂(60), 1%MoS₂/CdS-TiO₂(60) nanofibers; and CdS-TiO₂ nanofibers (inset).

in the visible light region with the increasing photodeposition time (inset in Fig. 2). It can be attributed to the increase amount of CdS in the as-prepared samples.

The morphologies of the as-fabricated products have been observed by SEM and TEM, as shown in Fig. 3, Fig. S2 and S3. For the CdS-TiO₂(60) samples, CdS nanoparticles are well distributed on the surface of TiO₂ nanofibers. Fig. 3a shows the TEM image of the as-prepared 1%MoS₂/CdS-TiO₂(60) nanofibers. After the photodeposition of MoS₂, the morphology of MoS₂/CdS-TiO₂(60) nanofibers is similar to CdS-TiO₂ nanofibers. The TEM image also exhibits that CdS nanoparticles supported on P25 are more inclined to agglomerate (Fig. S3). Therefore, compared to P25, the electrospun TiO₂ nanofibers as supports can effectively improve the dispersion of CdS nanoparticles. The high resolution TEM (HRTEM) image in Fig. 3b reveals that the lattice fringes of 0.35 nm and 0.33 nm can be assigned to the (101) lattice plane of anatase TiO₂ and (002) lattice plane of hexagonal CdS, respectively [40]. In addition, as shown in Fig. 3b, MoS₂ are hard to be distinguished due to the

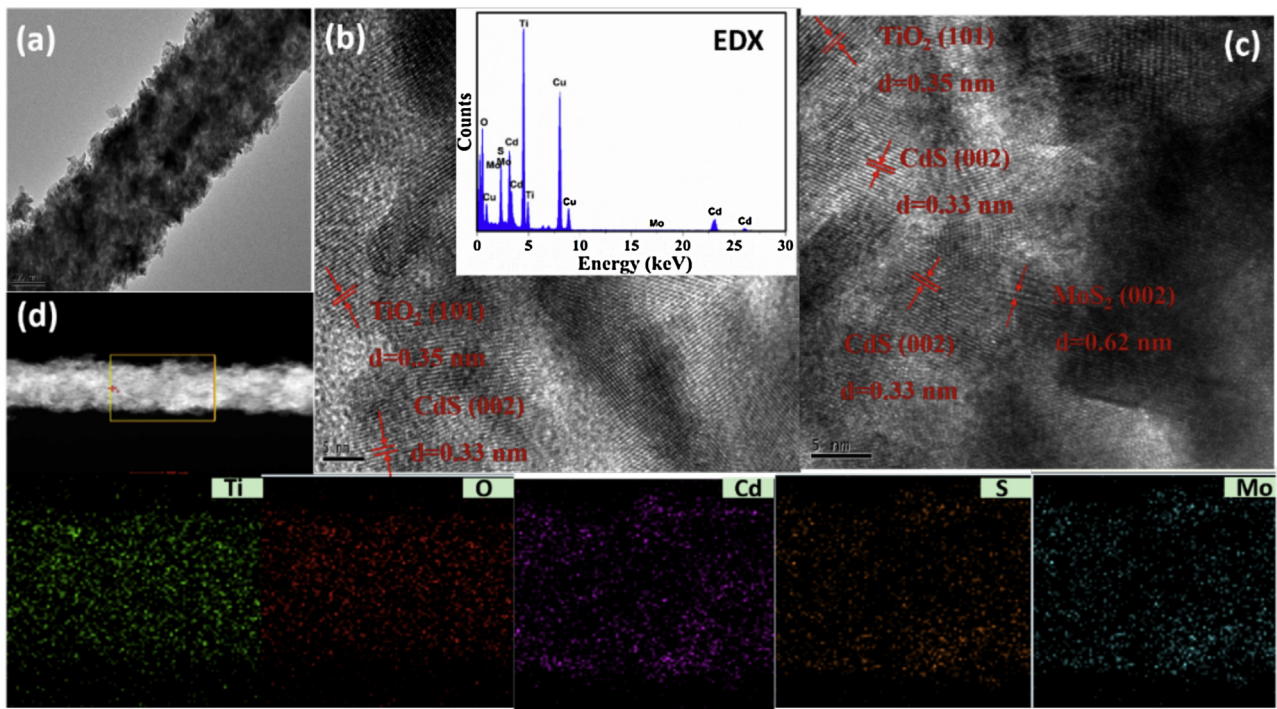


Fig. 3. TEM image (a), HRTEM image (b) and EDX of 1%MoS₂/CdS-TiO₂(60) nanofibers, and elemental mapping patterns of the selected area in (d); HRTEM image of 3%MoS₂/CdS-TiO₂(60) nanofibers (c).

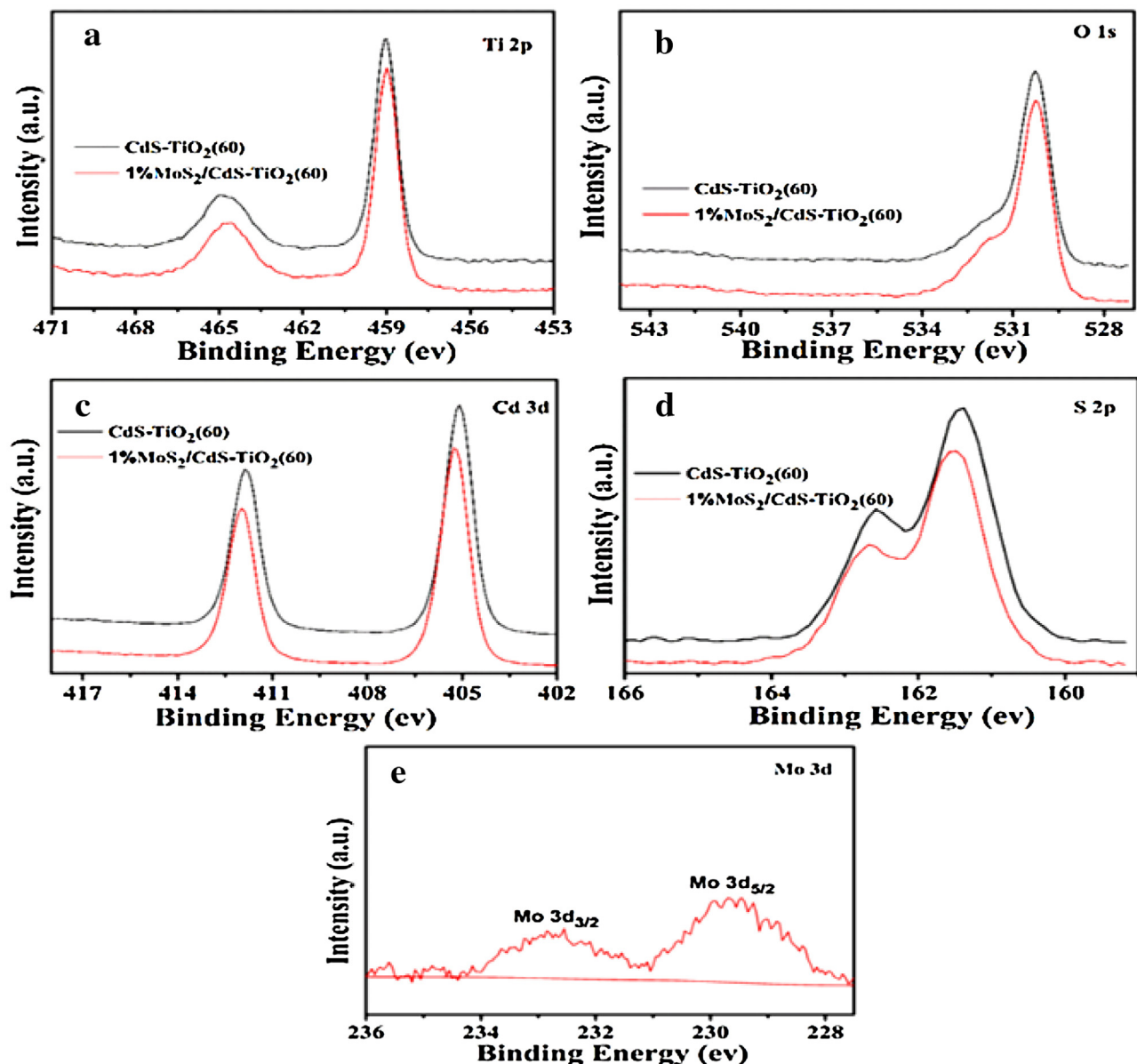


Fig. 4. XPS spectra of the CdS-TiO₂(60) and MoS₂/CdS-TiO₂(60): (a) Ti 2p, (b) O 1s, (c) Cd 3d, (d) S 2p, (e) Mo 3d, respectively.

low content or homogeneous dispersion of MoS₂. However, with the weight ratio increased to 3%, MoS₂ can be observed clearly. As shown in Fig. 3c and S4, clear lattice fringes of 0.62 nm coinciding with the (0 0 2) plane of hexagonal MoS₂ have appeared. Also, it has been reported that such kind of MoS₂ is highly active and versatile catalysts for the H₂ evolution reaction [46]. In addition, the energy-dispersive X-ray spectrometry (EDX) confirms the existence of Ti, O, Cd, Mo and S elements in the as-prepared 1%MoS₂/CdS-TiO₂(60) samples. The elemental mapping images further indicate that Ti, O, Cd, Mo and S elements are uniformly distributed on the 1D TiO₂ nanofibers. Therefore, to further confirm the chemical composition and the surface valence state of the sample, the XPS analysis has been performed.

The XPS spectra of the as-prepared CdS-TiO₂(60) and MoS₂/CdS-TiO₂(60) are shown in Fig. 4. The XPS peak for C 1s at 284.6 eV is ascribed to adventitious carbon from the XPS instrument. The introduction of MoS₂ has no obvious influence on the principal peak position of the Ti 2p and O 1s peaks. The peak centered at around 459.1 eV and 464.8 eV (Fig. 4a) are assigned to Ti 2p_{3/2} and Ti 2p_{1/2},

respectively [47]. The observed spin-orbit splitting between the Ti 2p_{3/2} and Ti 2p_{1/2} is ca. 5.7 eV, indicating the existence of the Ti⁴⁺ state in MoS₂/CdS-TiO₂(60) nanofibers. Two peaks at 405.2 and 411.8 eV (Fig. 4c) are assigned to Cd 3d_{5/2} and 3d_{3/2}, respectively [48]. Nevertheless, positive shifts of the binding energy of Cd 3d are exhibited at about 0.2 and 0.1 eV compared with CdS-TiO₂(60) nanofibers, which indicates a strong interaction between MoS₂ and CdS-TiO₂ nanofibers [49]. The peaks at 161.4 and 162.4 eV (Fig. 4d) in S 2p spectra are characteristic of the S²⁻ [49]. Moreover, the Mo 3d peaks at 229.4 and 232.5 eV (Fig. 4e) correspond to Mo 3d_{5/2} and Mo 3d_{3/2}, respectively, which indicate the presence of a +4 oxidation state of Mo in the sample of MoS₂/CdS-TiO₂(60) [38]. Nevertheless, compared the XPS spectra of MoS₂/CdS-TiO₂(60) with MoS₂/CdS-P25(60) (Fig. S5), positive shifts of the binding energy of Ti 2p and Mo 3d indicate the stronger interfacial contact among MoS₂, CdS and TiO₂ in MoS₂/CdS-TiO₂(60) sample. The XPS results further suggest that an intimate interfacial interaction between MoS₂ and CdS-TiO₂ nanofibers is beneficial for improving the transfer of photogenerated electrons during the photocatalysis.

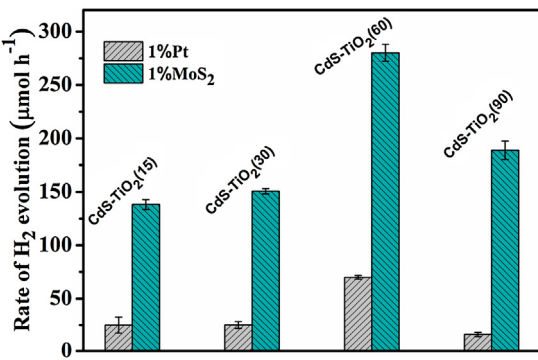


Fig. 5. Photocatalytic H₂ evolution rate over CdS-TiO₂ nanofibers loaded with 1%MoS₂ or 1%Pt. Conditions: catalyst 20 mg; H₂O 72 mL; lactic acid 8 mL; visible light ($\lambda \geq 420$ nm).

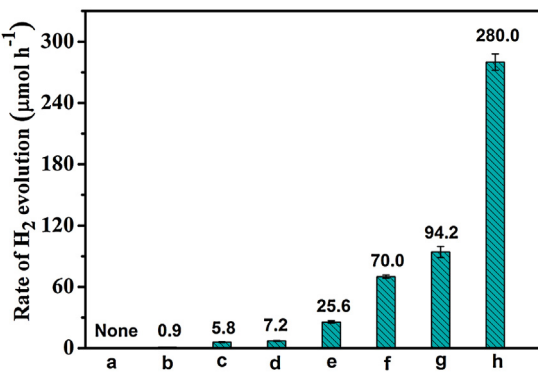


Fig. 6. Photocatalytic hydrogen evolution rate over (a) 1%MoS₂/CdS-TiO₂(60) in the dark; (b) 1%MoS₂/TiO₂; (c) CdS-P25(60); (d) CdS-TiO₂(60); (e) 1%Pt/CdS-P25(60); (f) 1%Pt/CdS-TiO₂(60); (g) 1%MoS₂/CdS-P25(60); (h) 1%MoS₂/CdS-TiO₂(60).

3.2. Photocatalytic performance

The photocatalytic H₂ evolution activity of the as-obtained samples have been investigated in the presence of lactic acid as the sacrificial under visible light irradiation ($\lambda \geq 420$ nm). As shown in Fig. 5, it is observed that the photoactivity trends are the same for two series samples of 1%Pt/CdS-TiO₂ and 1%MoS₂/CdS-TiO₂. The photoactivities are increased with the prolonged photodeposition time for CdS in the range of 15–60 min. For the samples with 90 min irradiation, the lower photoactivities can be attributed to the aggregation of CdS nanoparticles on the TiO₂ nanofibers surface, resulting in a reduced surface area, as shown in Table S1. It is noteworthy pointing out that among these prepared samples, the 1%MoS₂/CdS-TiO₂(60) exhibits the highest H₂ evolution rate of 280.0 μmol h⁻¹, corresponding to an apparent quantum efficiency (AQE) of 19.3% at 420 nm (see Fig. S6). These results further indicate that the photodeposition of MoS₂ on the CdS-TiO₂ nanofibers is a facile but effective method for the high photocatalytic H₂ evolution.

Fig. 6 shows the photocatalytic H₂ evolution activity under various experimental conditions. In the absence of light, no H₂ production is detected, suggesting that H₂ production is driven by the photocatalytic process. Loading 1%Pt can improve the performance. The photocatalytic H₂ evolution rate of 1%Pt/CdS-TiO₂(60) is 70.0 μmol h⁻¹, which is 2.7 times higher than that of 1%Pt/CdS-P25(60) (25.6 μmol h⁻¹). Considering the amounts of Cd determined by ICP are approximate for CdS-TiO₂(60) nanofibers and CdS-P25(60) composites (see Table S2). It shows that the electrospun TiO₂ nanofibers as supports can effectively improve the dispersion of CdS nanoparticles [50]. When 1%MoS₂ is introduced as a cocatalyst, the sample of 1%MoS₂/CdS-TiO₂(60) shows the best activity and the H₂ evolution capability for these

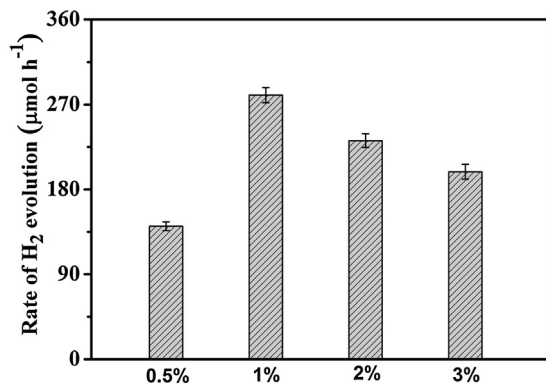


Fig. 7. Photocatalytic H₂ evolution rate over CdS-TiO₂(60) nanofibers with different amounts of MoS₂. Conditions: catalyst 20 mg; H₂O 72 mL; lactic acid 8 mL; visible light ($\lambda \geq 420$ nm).

samples follows the order: 1%MoS₂/CdS-TiO₂(60) > 1%MoS₂/CdS-P25(60) > 1%Pt/CdS-TiO₂(60) > 1%Pt/CdS-P25(60). Combining this results, the enhanced photocatalytic activity of 1%MoS₂/CdS-TiO₂(60) further indicates that both the composites interfacial contact and the unique architecture are beneficial to the transfer of photogenerated electrons. Because the electrospun TiO₂ nanofibers consisting of highly crystalline and closely interconnected TiO₂ nanoparticles are beneficial for the vectorial transfer of photogenerated charge carriers, leading to an effective separation of electron–hole pairs. Furthermore, the catalytic activity of the prepared CdS is also studied. As shown in Fig. S7, notably, the photocatalytic H₂ evolution rate of 1%MoS₂/CdS-TiO₂(60) nanofibers is much higher than the pure CdS, and about 1.8 times higher than 1%MoS₂/CdS. As a result, it can be conclude that, introducing the TiO₂ nanofibers greatly enhances the properties of CdS.

The effect of MoS₂ loading amount on the H₂ evolution rate is also investigated. The sample of CdS-TiO₂(60) is used as the substrate to prepare (X%)MoS₂/CdS-TiO₂(60) composites loaded with different MoS₂ contents (0.5–3 wt%). As shown in Fig. 7, the rate of H₂ evolution increases with increasing amount of MoS₂ from 0.5 to 1%. When the content of MoS₂ is 1 wt%, the obtained sample of 1%MoS₂/CdS-TiO₂(60) shows the highest photocatalytic hydrogen evolution rate of 280.0 μmol h⁻¹. Because the surface of the MoS₂ exists hydrogen active center, which can reduce the overpotential and improve the photocatalytic H₂ production [32]. However, further increasing the amount of MoS₂, it results a decrease in the photocatalytic activity. Such a decrease in the activities of samples is likely due to the shading effect of MoS₂ [51], which could block the light absorption of CdS.

The recoverability is also an important consideration for its practical application of a photocatalyst. XRD and XPS results reveal that the crystal structure and surface chemical compositions of 1%MoS₂/CdS-TiO₂(60) still keep unchanged before and after the photocatalytic reaction, respectively (see Figs. S8 and S9). Furthermore, the stability of 1%MoS₂/CdS-TiO₂(60) sample has been tested by using the same catalyst for photocatalytic H₂ production repeatedly four times (as shown in Fig. 8). After four recycles, no obvious loss of the activity can be observed, indicating the high stability of 1%MoS₂/CdS-TiO₂(60) during photocatalytic H₂ evolution. The remaining reaction solution after reuse was also centrifuged and analyzed with ICP. It shows that there is little Cd²⁺ leaching after photocatalytic process, indicating the good stability of 1%MoS₂/CdS-TiO₂(60) nanofibers.

To better understand the importance of interfacial contact among the composites on promoting the separation of electron–hole pairs and improving the photoactivity, we have characterized the photoelectrochemical analysis using the opti-

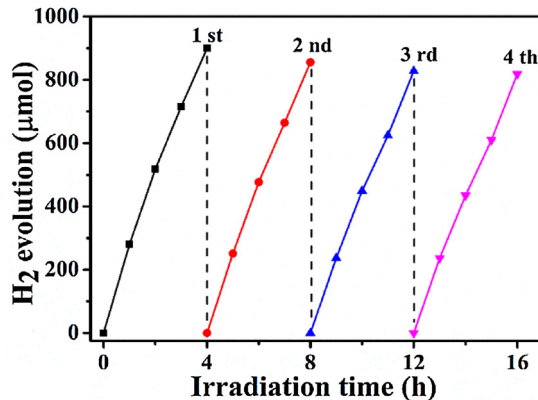


Fig. 8. Cycle runs for the photocatalytic H_2 production of 1% $\text{MoS}_2/\text{CdS-TiO}_2(60)$ nanofibers.

mum sample of 1% $\text{MoS}_2/\text{CdS-TiO}_2(60)$. As shown in Fig. 9a, under visible light irradiation, the transient photocurrent response for 1% $\text{MoS}_2/\text{CdS-TiO}_2(60)$ is much higher than that of 1% $\text{MoS}_2/\text{CdS-P25}(60)$ and $\text{CdS-TiO}_2(60)$, suggesting the more efficient separation of the photoexcited electron–hole pairs. To further determine the advantage, electrochemical impedance spectra (EIS) have also been performed. It can be seen from Fig. 9b that 1% $\text{MoS}_2/\text{CdS-TiO}_2(60)$ shows the smallest semicircle at high frequencies, indicating the more efficient separation of photogenerated charge carriers over 1% $\text{MoS}_2/\text{CdS-TiO}_2(60)$. It is clear that the interfacial charge transfer has a significant influence on the improvement of photocatalytic H_2 production. In addition, the most efficient separation and longest lifetime of photo-excited electron–hole pairs of 1% $\text{MoS}_2/\text{CdS-TiO}_2(60)$ have also been confirmed by the photoluminescence (PL) analysis. As shown in Fig. S10, we can find that the PL intensity of 1% $\text{MoS}_2/\text{CdS-TiO}_2(60)$ is the lowest among these three samples, which suggests that the recombination of electron–hole pairs photogenerated from 1% $\text{MoS}_2/\text{CdS-TiO}_2(60)$ is the most efficiently inhibited [52]. Furthermore, the time-resolved fluorescence decay spectra shows that 1% $\text{MoS}_2/\text{CdS-TiO}_2(60)$ exhibits a longer PL lifetime (~ 1.20 ns) than $\text{CdS-TiO}_2(60)$ (~ 1.01 ns) and 1% $\text{MoS}_2/\text{CdS-P25}(60)$ (~ 1.10 ns) (Fig. S10). It is believed that the increased lifetimes of charge carriers of 1% $\text{MoS}_2/\text{CdS-TiO}_2(60)$ are more efficient for photocatalytic applications.

A tentative mechanism for photocatalytic H_2 evolution over the $\text{MoS}_2/\text{CdS-TiO}_2$ nanofibers under visible light irradiation is shown in Fig. 10. Once the CdS is excited, the photo-generated holes are consumed by sacrificial regents and net photo-generated electrons

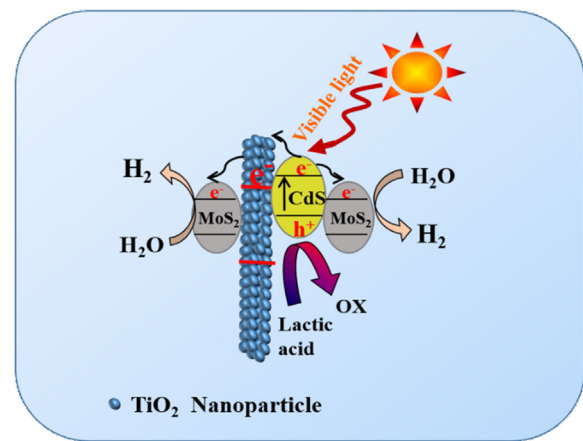


Fig. 10. Schematic illustration of $\text{MoS}_2/\text{CdS-TiO}_2$ nanofibers for photocatalytic H_2 evolution under the irradiation of visible light ($\lambda \geq 420$ nm).

are produced. The photo-generated electrons can not only directly transfer to the hydrogen evolution active sites on MoS_2 due to the intimate interfacial contacts, but also indirectly migrate to MoS_2 via the TiO_2 as the bridge because of the type II energy band structures between CdS and TiO_2 [53,54]. Thanks to the excellent performance of MoS_2 for promoting the hydrogen evolution, the photocatalytic hydrogen evolution activity over $\text{MoS}_2/\text{CdS-TiO}_2$ with this unique architecture enhances dramatically.

4. Conclusions

In summary, a facile, rapid and efficient electrospinning mediated photodeposition method has been developed to prepare $\text{MoS}_2/\text{CdS-TiO}_2$ nanofibers. The sample of 1% $\text{MoS}_2/\text{CdS-TiO}_2$ shows much higher photocatalytic activities for H_2 evolution than 1% $\text{Pt}/\text{CdS-TiO}_2$ nanofibers and 1% $\text{MoS}_2/\text{CdS-P25}$ composites under the same experiment conditions. It can be ascribed as follows: First of all, the electrospun TiO_2 nanofibers has advantages over the P25 nanoparticle as supports in improving the dispersion of CdS and MoS_2 ; in addition, the formed interfacial contact among composites can increase charge carrier transfer. Our current work could not only testify the significant influence of intimate interfacial contact on improving photocatalytic performance, but also enrich the facile fabrication of more efficient $\text{MoS}_2/\text{semiconductor}$ photocatalysts for photocatalytic H_2 evolution from water.

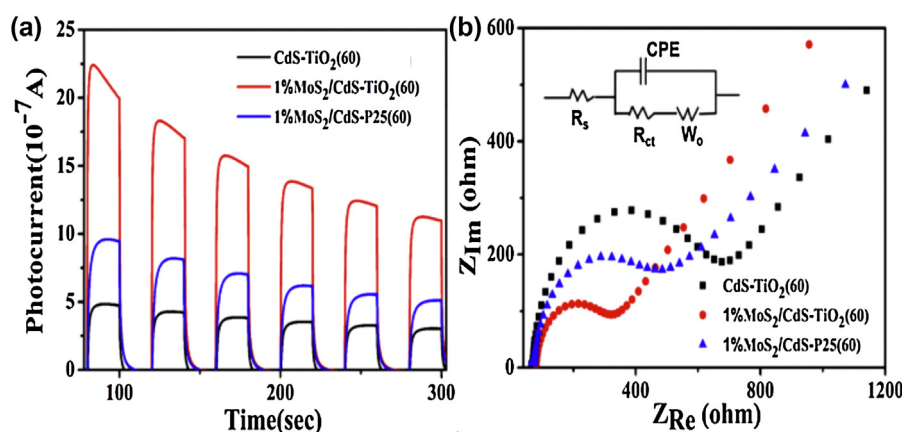


Fig. 9. (a) Transient photocurrent response of $\text{CdS-TiO}_2(60)$ nanofibers, 1% $\text{MoS}_2/\text{CdS-TiO}_2(60)$ nanofibers, and 1% $\text{MoS}_2/\text{CdS-P25}(60)$ composites under the irradiation of visible light ($\lambda \geq 420$ nm); (b) Electrochemical impedance spectra of $\text{CdS-TiO}_2(60)$ nanofibers, 1% $\text{MoS}_2/\text{CdS-TiO}_2(60)$ nanofibers, and 1% $\text{MoS}_2/\text{CdS-P25}(60)$ composites.

Acknowledgements

This work was supported by the National Natural Science Foundation of China (21273036 and 21177024) and the National Key Basic Research Program of China (2014CB239303).

Appendix A. Supplementary data

Supplementary data associated with this article can be found, in the online version, at <http://dx.doi.org/10.1016/j.apcatb.2016.09.040>.

References

- [1] J.W. Ha, T.P.A. Ruberu, R. Han, B. Dong, J. Vela, N. Fang, *J. Am. Chem. Soc.* 136 (2014) 1398–1408.
- [2] D.J. Martin, K. Qiu, S.A. Shevlin, A.D. Handoko, X. Chen, Z. Guo, J. Tang, *Angew. Chem. Int. Ed.* 53 (2014) 9240–9245.
- [3] X. Zhang, L. Yu, C. Zhuang, T. Peng, R. Li, X. Li, *ACS Catal.* 4 (2014) 162–170.
- [4] P. Niu, L. Zhang, G. Liu, H.M. Cheng, *Adv. Funct. Mater.* 22 (2012) 4763–4770.
- [5] Y.P. Xie, Z.B. Yu, G. Liu, X.L. Ma, H.-M. Cheng, *Energy Environ. Sci.* 7 (2014) 1895–1901.
- [6] A. Gasparotto, D. Barreca, D. Bekermann, A. Devi, R.A. Fischer, P. Fornasiero, V. Gombac, O.I. Lebedev, C. Maccato, T. Montini, *J. Am. Chem. Soc.* 133 (2011) 19362–19365.
- [7] X. Zong, H. Yan, G. Wu, G. Ma, F. Wen, L. Wang, C. Li, *J. Am. Chem. Soc.* 130 (2008) 7176–7177.
- [8] Y. Yin, Z. Jin, F. Hou, *Nanotechnology* 18 (2007) 495608–495700.
- [9] Y. Li, L. Tang, S. Peng, Z. Li, G. Lu, *CrystEngComm* 14 (2012) 6974–6982.
- [10] A. Kudo, Y. Miseki, *Chem. Soc. Rev.* 38 (2009) 253–278.
- [11] J. Yang, D. Wang, H. Han, C. Li, *Acc. Chem. Res.* 46 (2013) 1900–1909.
- [12] K. Chang, Z. Mei, T. Wang, Q. Kang, S. Ouyang, J. Ye, *ACS Nano* 8 (2014) 7078–7087.
- [13] V.M. Dascalaki, M. Antoniadou, G. Li Puma, D.I. Kondarides, P. Lianos, *Environ. Sci. Technol.* 44 (2010) 7200–7205.
- [14] H. Yan, J. Yang, G. Ma, G. Wu, X. Zong, Z. Lei, J. Shi, C. Li, *J. Catal.* 266 (2009) 165–168.
- [15] H. Zhao, Y. Dong, P. Jiang, G. Wang, H. Miao, R. Wu, L. Kong, J. Zhang, C. Zhang, *ACS Sustain. Chem. Eng.* 3 (2015) 969–977.
- [16] Y. Xu, W. Zhao, R. Xu, Y. Shi, B. Zhang, *Chem. Commun.* 49 (2013) 9803–9805.
- [17] N. Bao, L. Shen, T. Takata, K. Domen, *Chem. Mater.* 20 (2007) 110–117.
- [18] L. Shen, M. Luo, Y. Liu, R. Liang, F. Jing, L. Wu, *Appl. Catal. B: Environ.* 166 (2015) 445–453.
- [19] R. Lin, L. Shen, Z. Ren, W. Wu, Y. Tan, H. Fu, J. Zhang, L. Wu, *Chem. Commun.* 50 (2014) 8533–8535.
- [20] Y. Chen, L. Wang, G.M. Lu, X. Yao, L. Guo, *J. Mater. Chem.* 21 (2011) 5134–5141.
- [21] L. Wu, F. Li, Y. Xu, J.W. Zhang, D. Zhang, G. Li, H. Li, *Appl. Catal. B: Environ.* 164 (2015) 217–224.
- [22] S. Banerjee, S.K. Mohapatra, P.P. Das, M. Misra, *Chem. Mater.* 20 (2008) 6784–6791.
- [23] Y.J. Hwang, S. Yang, E.H. Jeon, H.W. Nho, K.-J. Kim, T.H. Yoon, H. Lee, *Appl. Catal. B: Environ.* 180 (2016) 480–486.
- [24] Z. Zhang, C. Shao, X. Li, Y. Sun, M. Zhang, J. Mu, P. Zhang, Z. Guo, Y. Liu, *Nanoscale* 5 (2013) 606–618.
- [25] Y. Shengyuan, A.S. Nair, R. Jose, S. Ramakrishna, *Energy Environ. Sci.* 3 (2010) 2010–2014.
- [26] H.-i. Kim, S. Kim, J.-K. Kang, W. Choi, *J. Catal.* 309 (2014) 49–57.
- [27] C. Luo, S.D. Stoyanov, E. Stride, E. Pelan, M. Edirisinghe, *Chem. Soc. Rev.* 41 (2012) 4708–4735.
- [28] M. Shang, W. Wang, W. Yin, J. Ren, S. Sun, L. Zhang, *J. Chem. Eur.* 16 (2010) 11412–11419.
- [29] G. Li, L. Wu, F. Li, P. Xu, D. Zhang, H. Li, *Nanoscale* 5 (2013) 2118–2125.
- [30] M. Nguyen, P.D. Tran, S.S. Pramana, R.L. Lee, S.K. Batabyal, N. Mathews, L.H. Wong, M. Graetzel, *Nanoscale* 5 (2013) 1479–1482.
- [31] J. Zhang, J. Yu, M. Jaroniec, J.R. Gong, *Nano Lett.* 12 (2012) 4584–4589.
- [32] Q. Xiang, J. Yu, M. Jaroniec, *J. Am. Chem. Soc.* 134 (2012) 6575–6578.
- [33] T.F. Jaramillo, K.P. Jørgensen, J. Bonde, J.H. Nielsen, S. Horch, I. Chorkendorff, *Science* 317 (2007) 100–102.
- [34] J. Xiong, Y. Liu, D. Wang, S. Liang, W. Wu, L. Wu, *J. Mater. Chem. A* 3 (2015) 12631–12635.
- [35] T. Jia, A. Kolpin, C. Ma, R.C.-T. Chan, W.-M. Kwok, S.E. Tsang, *Chem. Commun.* 50 (2014) 1185–1188.
- [36] W. Zhou, Z. Yin, Y. Du, X. Huang, Z. Zeng, Z. Fan, H. Liu, J. Wang, H. Zhang, *Small* 9 (2013) 140–147.
- [37] D. Kong, H. Wang, J.J. Cha, M. Pasta, K.J. Koski, J. Yao, Y. Cui, *Nano Lett.* 13 (2013) 1341–1347.
- [38] Y. Li, H. Wang, L. Xie, Y. Liang, G. Hong, H. Dai, *J. Am. Chem. Soc.* 133 (2011) 7296–7299.
- [39] D. Li, Y. Xia, *Nano Lett.* 3 (2003) 555–560.
- [40] X. Pan, Y.-J. Xu, *J. Phys. Chem. C* 119 (2015) 7184–7194.
- [41] S. Kanda, T. Akita, M. Fujishima, H. Tada, *J. Colloid Interface Sci.* 354 (2011) 607–610.
- [42] W. Ho, J.C. Yu, J. Lin, J. Yu, P. Li, *Langmuir* 20 (2004) 5865–5869.
- [43] J. Xu, Y. Li, S. Peng, *Int. J. Hydrogen Energy* 40 (2015) 353–362.
- [44] L. Wei, Y. Chen, Y. Lin, H. Wu, R. Yuan, Z. Li, *Appl. Catal. B: Environ.* 144 (2014) 521–527.
- [45] X. Chen, S. Shen, L. Guo, S.S. Mao, *Chem. Rev.* 110 (2010) 6503–6570.
- [46] Y. Li, H. Wang, S. Peng, *J. Phys. Chem. C* 118 (2014) 19842–19848.
- [47] Y. Huo, X. Yang, J. Zhu, H. Li, *Appl. Catal. B: Environ.* 106 (2011) 69–75.
- [48] L. Wu, C.Y. Jimmy, X. Fu, *J. Mol. Catal. A: Chem.* 244 (2006) 25–32.
- [49] Z. Lian, P. Xu, W. Wang, D. Zhang, S. Xiao, X. Li, G. Li, *ACS Appl. Mater. Interfaces* 7 (2015) 4533–4540.
- [50] M. Zhang, C. Shao, Z. Guo, Z. Zhang, J. Mu, T. Cao, Y. Liu, *ACS Appl. Mater. Interfaces* 3 (2011) 369–377.
- [51] Y. Hou, A.B. Laursen, J. Zhang, G. Zhang, Y. Zhu, X. Wang, S. Dahl, I. Chorkendorff, *Angew. Chem. Int. Ed.* 52 (2013) 3621–3625.
- [52] M.-Q. Yang, C. Han, Y.-J. Xu, *J. Phys. Chem. C* 119 (2015) 27234–27246.
- [53] G.-S. Li, D.-Q. Zhang, J.C. Yu, *Environ. Sci. Technol.* 43 (2009) 7079–7085.
- [54] Y. Hou, B.L. Abrams, P.C. Vesborg, M.E. Björketun, K. Herbst, L. Bech, A.M. Setti, C.D. Damsgaard, T. Pedersen, O. Hansen, *Nat. Mater.* 10 (2011) 434–438.